

# We are IntechOpen, the world's leading publisher of Open Access books Built by scientists, for scientists

4,500

Open access books available

119,000

International authors and editors

135M

Downloads

Our authors are among the

154

Countries delivered to

TOP 1%

most cited scientists

12.2%

Contributors from top 500 universities



WEB OF SCIENCE™

Selection of our books indexed in the Book Citation Index  
in Web of Science™ Core Collection (BKCI)

Interested in publishing with us?  
Contact [book.department@intechopen.com](mailto:book.department@intechopen.com)

Numbers displayed above are based on latest data collected.  
For more information visit [www.intechopen.com](http://www.intechopen.com)



# Real-time Physical Simulation of Wind Energy Conversion Systems

Iulian Munteanu<sup>1,2</sup>, Antoneta Iuliana Bratcu<sup>1,2</sup>,  
Seddik Bacha<sup>1</sup> and Daniel Roye<sup>1</sup>

<sup>1</sup>*Grenoble Electrical Engineering Laboratory (G2Elab),  
BP 46, 38402 Saint-Martin d'Hères*

<sup>2</sup>*"Dunărea de Jos" University of Galați,  
47 Domnească, 800008- Galați*

<sup>1</sup>*France*

<sup>2</sup>*Romania*

## 1. Introduction

The real-time wind turbine simulators are enabling the testing of wind energy conversion systems' (WECS) control units and of the associated control algorithms in a controlled environment. It is known that a simulator can predict the behaviour of an industrial system subjected to certain operating conditions before its real-world implementation. But, the main motivation of using physical simulators for wind energy applications, resides within another argument. It is about the fact that a dedicated laboratory setup can provide something that does not exist in real-world applications: controllable wind velocity. So, a wind turbine physical simulator offers a prime mover which behaves as a "wind-turbine-powered-like shaft" (Nichita et al., 2002), allowing the static and dynamic characteristics replication of a mathematically-modelled wind turbine. This is the great advantage of such simulator as it replaces very expensive parts – such as the turbine rotor and the drive train – operating in a stochastic environment by conveniently-controlled electrical motors, operating in a controlled environment. This allows the repetitive experiments being carried out independently from wind and meteorological conditions in a most safe laboratory environment. Besides its prime mover, all of the physical WECS elements are present in the physical simulator as they are in the real-world application. Therefore, the electromechanical part of the generation chain exhibits the real phenomena presented in a wind power system. In this way the above-listed advantages are not faded by replicating a simplified electrical behaviour and a WECS-dedicated control unit will interact with a genuine wind power system.

When analyzing the concerned literature, one can note that the preliminary experimental validation of WECS control laws is always performed on wind turbine simulators. This is a reason for quite rich literature being dedicated to this subject. One can find two types of papers dealing with small-scale WECS simulators for different generation configurations. The first category is composed of works focusing on test rig building aspects (Leithead et al., 1994; Battaioto et al., 1996; Rodriguez-Amenedo et al., 1998; Diop et al., 1999a; Akhmatov et

Source: Wind Power, Book edited by: S. M. Muyeen,  
ISBN 978-953-7619-81-7, pp. 558, June 2010, INTECH, Croatia, downloaded from SCIYO.COM

al., 2000; Cardenas et al., 2001; Rabelo & Hofmann, 2002; Teodorescu & Blaabjerg, 2004; Steurer et al., 2004). Some works underlining the role of test rigs for preliminary validation of WECS control laws compose a second category (Enslin & van Wyk, 1992; Cárdenas et al., 1996; Kana et al., 2001; Munteanu et al., 2005; Camblong et al., 2006; Munteanu et al., 2008b). One should note that the list is far from being exhausted.

This chapter aims at providing the reader with possible answers to the questions related to the manner in which a WECS physical simulator can be build, including implementation details about how its different elements must be chosen and how its effectiveness can be assessed. All these issues are dealt with in the next section. The third section contains a comprehensive example in the form of a case study that applies the theoretical guidelines introduced previously. The last section, the fourth, is dedicated to conclusion. The chapter is completed by an appendix section. Even if this chapter concerns mainly the physical simulation of the horizontal-axis wind turbines (HAWT), the presented principles can be used without significant changes for the vertical-axis wind turbines.

## 2. How to build a WECS simulator?

### 2.1 Concepts

This section mainly refers to the prime mover rebuilding (in the sense of its behaviour replication), whereas the other parts are assembled by using the same methods and equipment as in the real-world application. As already stated, the turbine rotor should be replaced by an electrical servomotor which behaves as the former. To fulfil that purpose, the electrical motor is somehow driven by the wind turbine mathematical model, provided that an adequate model is available.

Of course that the entire simulator can be built using only hardware elements (*i.e.*, by using analogic integrated circuits for implementing the turbine model), but taking into account the computing power of the digital systems, the turbine model is implemented as software in the quasi-totality of the cases. Therefore, the WECS simulator has a physical part – which develops power – and a software part – the controlling model – connected in closed loop.

Conceptually speaking, a system containing a software model interacting directly with a hardware control unit has emerged in the last years as hardware-in-the-loop (HIL) simulator (Hanselmann, 1996). It is clear that the two closed-loop subsystems exchange only information one with each other. This kind of system has been extensively used for developing (fast prototyping) and testing control structures for mechanical equipments.

Concerning the WECS simulator, the interaction between the simulated plant (turbine aerodynamics) and the physical part (servomotor) suppose not only the information transfer but also the existence of the associated physical variables, as the servomotor develops power. This version of the concept is often called power hardware-in-the-loop (PHIL) simulation (Wu et al., 1996). The main difference with respect to the original concept is the existence of a power interface between the simulated plant and the so-called hardware under test. Even if the WECS physical simulator finds itself in the PHIL category, for sake of simplicity the term HIL will be used in the following.

### 2.2 Methodology

The simulator building approach presented in this work relies upon the general concepts, terminology and methodological aspects introduced by Nichita et al. (1998) and reused in Munteanu et al. (2008a). Even if it is dedicated entirely to the WECS simulators, the present

text uses some more general concepts and variables, which are valid for an entire class of industrial systems (Andreica et al., 2009).

Beside the WECS to be simulated, one must define an associated class of the operating conditions to be analyzed or of the control problems to be solved. Correspondingly, one can generally consider suitable input and output vectors (e.g., the wind velocity and the output power), as Figure 1 depicts. Irrespectively of the actual WECS configuration, the intended analysis is focused on a precise subsystem, denoted in the HIL-related literature as *hardware under test*. So, the basic idea used in HIL structures generally supposes that the original plant can be naturally divided into two subsystems which interact one with the other. Generally speaking, the two subsystems are chosen in order to fulfil some simulation efficiency criterion. In most of the cases, the first subsystem is such that the closed loop experiments are very expensive and deterministic experiments are almost impossible and it represents the prime mover. Therefore, it will be this subsystem whose behaviour must be replaced by a physical simulator; consequently, it will be called an *emulated physical system* (EPS). This implies that EPS is the only part of the plant that is mandatory to model. In the WECS case, this can be the turbine rotor and can include the drive train. The second subsystem will exist in the HIL simulator exactly as it is in the original plant, thus allowing laboratory experiments under realistic conditions. Being the object of research undertaking the control action, it will be further called in this text an *investigated physical system* (IPS).

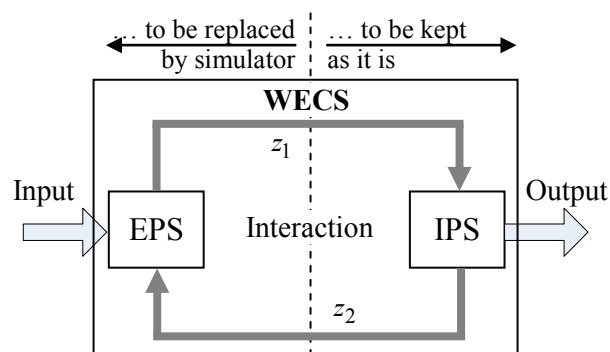


Fig. 1. Original plant to simulate illustrating the interaction between the IPS and the EPS

The interaction between EPS and IPS, corresponding to a power transfer between them, is characterized by a pair of so-called *interaction variables*, further denoted as  $z_1$  and  $z_2$ .

Supposing that the EPS is the prime mover, the energy flows towards IPS. Having made this assumption, the interaction from the EPS point of view is depicted in Figure 1. The physical nature of the interaction variables depends on the original system in a biunique manner.  $z_1$  is the cause variable, whose variation initiates the energy imbalance, and  $z_2$  is the response variable, common to the EPS and IPS. By virtue of their coupling, their product has always power dimension.

Now, concerning the WECS physical simulation, in the quasi-totality of cases available in the literature, the building of an electro-mechanical simulator is intended. Hence, the WECS is split between EPS and IPS at one of its rotating shafts. So, the two interaction variables are the shaft torque and the rotational speed, and EPS will contain at least the aerodynamics subsystem. This is not, of course, the sole simulator configuration that can be chosen.

The solution employed to build a physical simulator is to replace the EPS by the so-called *real-time physical simulator* (RTPS). The IPS remains the same as in the WECS, as its

behaviour study represents one of the main purposes of the HIL simulator building. The RTPS must offer the “natural” environment for IPS and must replicate the EPS behaviour and the interaction EPS-IPS. In this way the resulted HIL simulator will approximate the original WECS dynamics. In short, the RTPS must physically provide one of the interaction variables based on the measure of the other one and, of course, on the EPS model. This goal is achieved by means of a tracking loop at the output of the RTPS, which in some works (Munteanu, 2006) is called the *effector* (EFTs in Figure 2); the controlled variable is called driving variable and the measured one – response variable.

The effector reference is established by a model of the EPS; its input is established by an algorithm dedicated to the resource synthesis (e.g., wind speed). This model is embedded as software subsystem in the so-called *real-time software simulator* (RTSS). In conclusion, the RTPS includes the real-time software simulator (EPS modelling) and the tracking loop for physical replication of the controlled interaction variable. This structure is given in Figure 2.

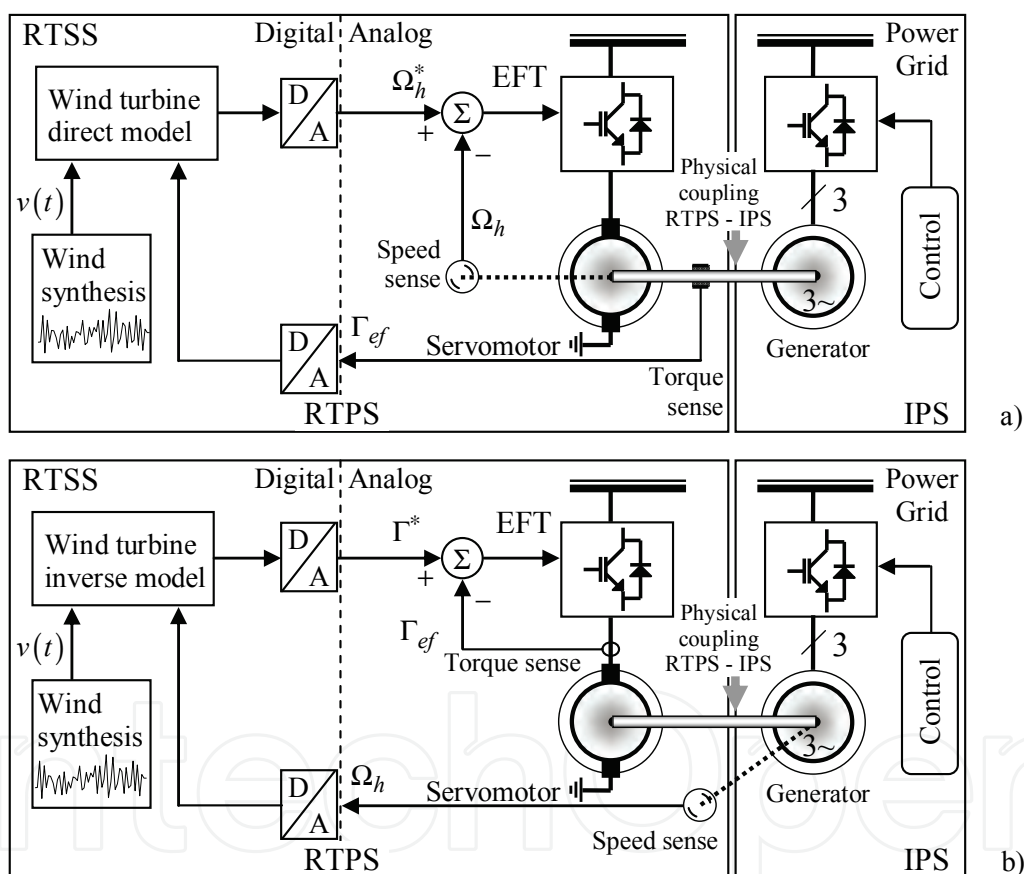


Fig. 2. Example of WECS HIL electromechanical simulator structures: a) the driving variable is an effect; b) the driving variable is a cause

When choosing the driving and response variables, two situations may happen, as follows. Let us consider a first case, when the driving variable is an output or a state of the WECS. So, it is about controlling an effect variable (of  $z_2$  type), and the model implemented in the RTSS is strictly causal and is obtained directly from the EPS model, fed by a measure of the cause variable ( $z_1$ ). For example, this effect variable can be a rotational speed if it is about an electromechanical simulator or a voltage if it is about an electrical simulator. An example is given in Figure 2a). There is also a second case when the driving variable is a cause variable



(of  $z_1$  type). In this event, the model implemented in the RTSS is non-causal (the EPS inverse model) and is fed by a measure of the effect,  $z_2$ . This effect variable can be a mechanical torque in an electromechanical HIL simulator and the associated software implementation implies the EPS model being rewritten. An example is given in Figure 2b).

Both of the two above-described cases have disadvantages, which can affect the simulator reliability. In the first case the effector dynamic is quite slow, whereas getting the second case into practice is difficult because temporal derivatives must be computed, increasing the measurement noise. Also, in Figure 2 one can note that the response variable is affected by the transducer dynamic and the driving variable by the effector dynamic. Therefore, these variables have slightly modified instantaneous values, affecting the accuracy with which the HIL simulator emulates the WECS. Of course that for ensuring good simulator performance, these dynamics, together with the computation inside the RTSS, must be sufficiently faster than the dynamic of the EPS.

As stated before, there is not just a single way of building HIL simulators for WECS. Usually – and it is also the case chosen in this chapter – it is considered that IPS and EPS interact by means of the rotating high-speed shaft. Thus, the RTPS physical part is based on a rotating electrical machine (servomotor), either DC motors (Battaioto et al., 1996; Rabelo et al., 2004), or AC machines offering similar performances (Steurer et al., 2004; Munteanu et al., 2005).

The IPS is typically based on synchronous or induction machine and may include power electronics converters and control systems in order to implement the variable-speed operation. The interaction variables in this case are the rotational speed,  $\Omega_h \equiv z_2$ , and the mechanical “effective” torque of the high-speed shaft,  $\Gamma_{ef} \equiv z_1$ , with the high-speed shaft dynamical characteristic being the RTPS output. The EPS consists of aerodynamics and drive train. The algorithm within RTSS will thus implement the associated models and also the wind velocity as a stochastic sequence with statistical parameters depending on a certain wind site. Models of various deterministic test signals can also be implemented.

In the speed-driven case, a measure of the high-speed shaft torque is required. A computed value of the generator electromagnetic torque is often preferred in this case (Munteanu et al., 2008b). In the torque-driven case, the effector needs a torque feedback. In most of cases a measure of the servomotor electromagnetic torque is available starting from currents measure (*e.g.*, the armature current in the case of a DC motor).

To conclude, between the two above-described cases one can remark some differences. Concerning the software, the aerodynamics model is inversed in the torque-driven case, while in the speed-driven case it is written “as is” in the RTSS. The associated hardware (effector) is configured as follows. The torque-driven case has a single control level – the very fast servomotor current (torque) loop. In the other case, there is a supplementary outer speed control loop; the speed controller should impose sufficiently fast dynamics to the coupling servomotor-generator in order to ensure sufficiently small simulation errors. In the following some more in-depth simulator building aspects will be presented.

### 2.3 Rigid drive train case

As stated before, a preliminary EPS short modelling stage is necessary. The aerodynamic subsystem of a fixed-pitch HAWT can be modelled in average by means of the interaction between air masses and the turbine rotor (Burton et al., 2001). The turbine model outputs the wind torque based on the wind velocity,  $v$ , and the low-speed shaft rotational speed,  $\Omega_l$ . The rotor aerodynamic performance is generally described by means of the power coefficient,  $C_p$ ,

which is a unimodal function of the tip speed ratio (Figure 3a), if assuming constant parameters of the air stream (air density, Reynolds numbers, *etc.*). If  $R$  denotes the blade length, the tip speed ratio is defined as:

$$\lambda = \Omega_i \cdot R / v \quad (1)$$

The  $C_p$  curve is constant for fixed-pitch turbines. When the wind speed varies, the power curves shapes reproduce the  $C_p$  shape (Wilkie et al., 1990), as shown in Figure 3b).

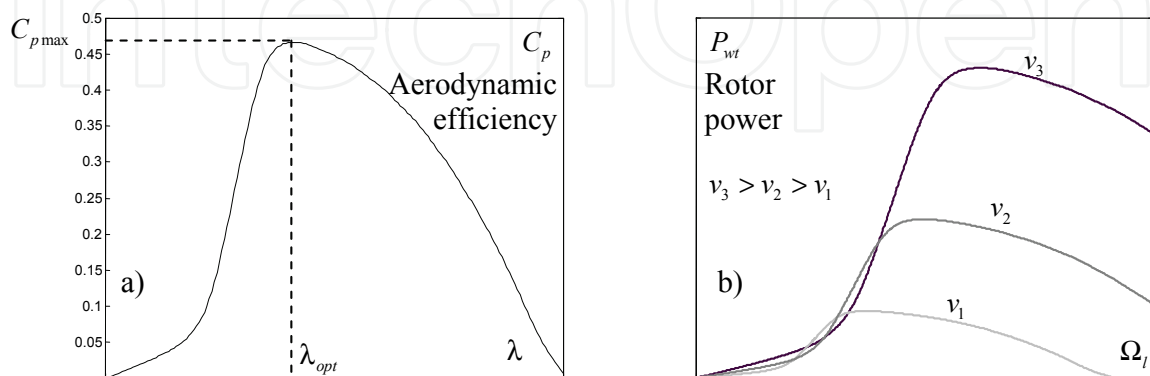


Fig. 3. a) Efficiency and b) corresponding power characteristics for a HAWT-based WECS  
The corresponding wind torque is given by the relation (Wilkie et al., 1990):

$$\Gamma_{wt}(\Omega_i, v) = 0.5 \cdot \pi \cdot \rho \cdot v^2 \cdot R^3 \cdot C_T(\lambda) + \Gamma_{ts} - \Gamma_{fv} - \Gamma_s, \quad (2)$$

where  $C_T(\lambda) = C_p(\lambda)/\lambda$  denotes the torque coefficient,  $\Gamma_{ts}$  represents the torque generated by the tower shadow effect,  $\Gamma_{fv}$  is the viscous friction torque and  $\Gamma_s$  is the static friction torque. Other elements can be added into relation (2), for example dynamical effects such as induction lag or spatial filter, in order to obtain a better approximation whenever needed (Rodriguez-Amendedo et al., 1998). If the turbine blades are pitchable, the wind torque is computed based on a supplementary input variable - the blades pitch,  $\beta$  -  $\Gamma_{wt}(\Omega_i, v, \beta)$ . The drive train is the interaction device between the turbine rotor and the electrical generator. A rigid drive train generally consists of a multistage helical or spur gear-based speed multiplier (together with the associated shafts), modelled in average by a multiplication ratio  $i$  and efficiency  $\eta$ . For modelling purposes, the dynamics of the rigid drive train are rendered either at the low-speed or at the high-speed shaft, thus obtaining the so-called one-mass model (Wilkie et al., 1990). The motion equation for the latter case is:

$$J_h \cdot \dot{\Omega}_h = \Gamma_R(v, \Omega_h) - \Gamma_G(\Omega_h), \quad (3)$$

where  $\Omega_h = i \cdot \Omega_i$  is the high-speed shaft rotational speed,  $\Gamma_R = \eta \cdot \Gamma_{wt}/i$  is the high-speed shaft torque and  $\Gamma_G$  is the electromagnetic torque provided by the electrical generator. The turbine inertia rendered at the high-speed shaft is  $J_h \approx J_{wt} \cdot \eta/i^2 + J_G$ , with  $J_{wt}$  and  $J_G$  being the turbine rotor and electrical generator inertias respectively. Relations (2) and (3) compose a model of the EPS.

Now, being given a test rig composed of a rigid coupling servomotor-generator with an inertia  $J_{sim} = J_G + J_{SM}$ , its associated motion equation can be written:

$$J_{sim} \cdot \dot{\Omega}_{sim} = \Gamma_{SM} - \Gamma_G(\Omega_h), \tag{4}$$

where  $\Gamma_{SM}$  and  $J_{SM}$  are the servomotor torque and inertia and  $\Omega_{sim}$  is its rotational speed. One wants that this mechanical assembly (simulator) rotates exactly as the WECS described by (3) when subjected to the same generator torque,  $\Gamma_G$ . Therefore, it is imposed that

$\Omega_{sim} \equiv \Omega_h$  and  $\dot{\Omega}_{sim} \equiv \dot{\Omega}_h$ . By subtracting equations (4) and (3), one obtains the necessary value of the servomotor torque for fulfilling the above conditions:

$$\Gamma_{SM}^* = \Gamma_R(v, \Omega_{sim}) - (J_h - J_{sim}) \cdot \dot{\Omega}_{sim} \tag{5}$$

Equation (5) shows that the torque value imposed to the servomotor is computed by subtracting the dynamical torque from the wind torque (at the high-speed shaft). The former variable is computed by estimating the simulator rotational speed gradient. The latter variable is calculated using a synthesized value of the wind speed, a measure of the simulator rotational speed and the model from (2). So, equation (5), together with a wind speed model, is to be implemented into RTSS for the torque-driven case (see Figure 4a).

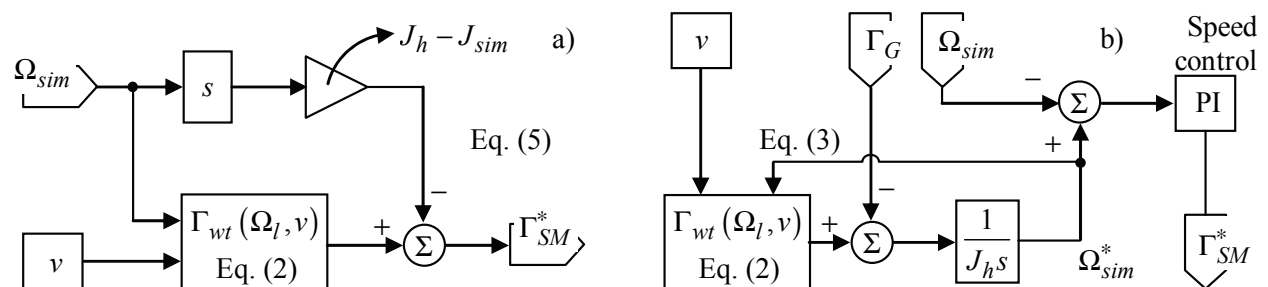


Fig. 4. RTSS configuration for WECS having rigid drive train: a) torque-driven case, b) speed-driven case

If a speed-driven scheme is required, one must impose to the servomotor-generator assembly the rotational speed value computed by integrating equation (3). Of course that a measure of the generator torque,  $\Gamma_G$ , should be available. The structure to implement, when the simulator speed controller is also embedded into the RTSS, is sketched in Figure 4b).

From a systemic viewpoint, the electromechanical part of WECS can be regarded as having two inputs, the wind speed and the electromagnetic (generator) torque, and one output, the rotational speed. Therefore, both wind speed and electromagnetic torque influence the rotational speed through two different channels (with different dynamics). The two above-described simulator structures should replicate the WECS behaviour for both influence channels. The simulation performances can be qualitatively assessed in the frequency domain if considering the linearized model of WECS around a typical operating point.

Figure 5 shows the relative position of the simulator characteristics with respect to the original WECS, for the two cases (torque- and speed-driven) and for both influence channels: the wind speed to rotational speed channel (Figure 5a) and the generator torque to rotational speed channel (Figure 5b). The influence of each channel has been studied independently of the other channel. These characteristics have been obtained by numerical simulation for a linearized low-power WECS, and do not contain the additional lags



induced by transducers, neither the simulation time step itself. Only the servomotor torque loop dynamics have been considered. Globally, one remarks that the simulation is valid until certain frequency. This value depends on the actual parameters of the rotational speed gradient estimator (see Figure 4a) and on those of the rotational speed controller (Figure 4b).

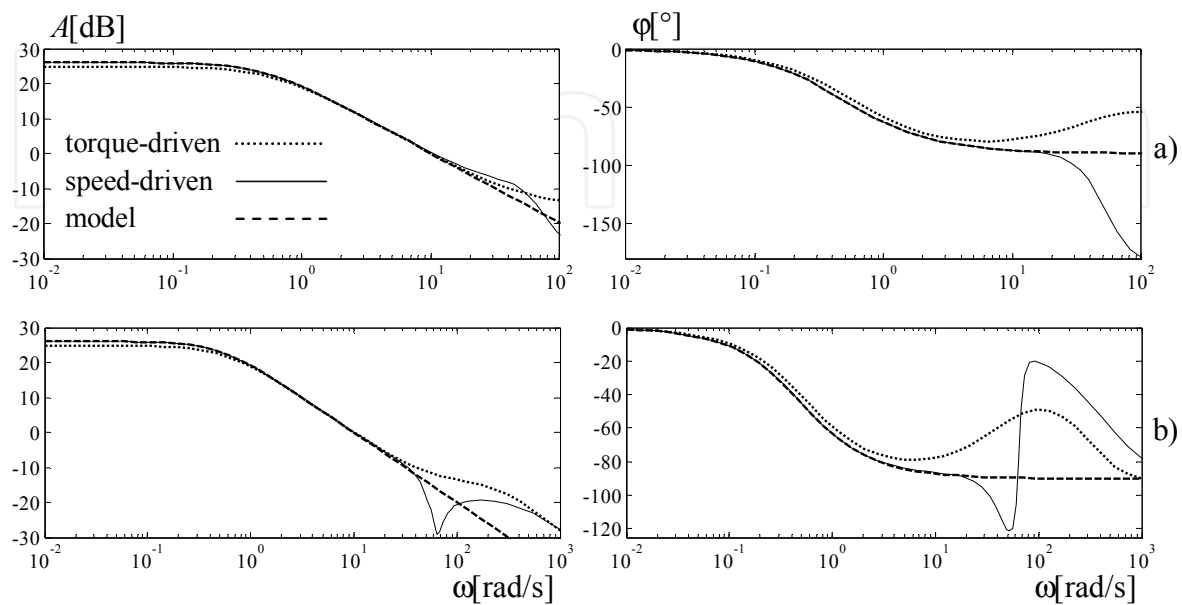


Fig. 5. The simulator frequency characteristics versus the original WECS model (dashed – model, solid – speed-driven case, dotted – torque-driven case): a) wind speed to rotational speed transfer, b) electromagnetic torque to rotational speed transfer

When analyzing Figure 5a), concerning the torque-driven case, one can remark a steady-state error in the gain, due to the nonzero dynamic friction of the simulator shaft. This means that a slight difference from the WECS rotational speed may appear, and may change with the operating point. For the same case, one can also note the leading effect in the phase characteristic, meaning that the high-frequency wind variations (turbulence) will not reproduce correctly the genuine rotational speed variations. However, the inherent lags present when a physical implementation is achieved can alleviate this aspect.

As regards Figure 5b), the characteristics have been traced for a larger frequency domain as the input torque variations can be significantly faster than the wind speed turbulences. For the torque-driven case one can restate the remarks above. For the speed-driven case one may expect bandwidth reduction when physical implementation is achieved. This figure lays out some limitations, particularly if the simulator is intended to be used as a WECS control laws benchmark. As the generator torque is the control input, one should not test WECS controllers designed with too large bandwidths. Otherwise, the designed controllers cannot be directly transferred to the real-world applications.

#### 2.4 Flexible drive train case

The same aerodynamic subsystem as in the rigid drive train case is considered; therefore the same model can be used. The flexible drive train dynamics are described by the following equations (Akhmatov, 2003):

$$\begin{cases} \dot{\Omega}_l = 1/J_{wt} \cdot \Gamma_{wt}(\Omega_l, v) - i/(\eta \cdot J_{wt}) \cdot \Gamma \\ \dot{\Omega}_h = 1/J_G \cdot \Gamma - 1/J_G \cdot \Gamma_G \\ \dot{\Gamma} = K_s(i\Omega_l - \Omega_h) + B_s(i\dot{\Omega}_l - \dot{\Omega}_h) \end{cases}, \quad (6)$$

where  $K_s$  and  $B_s$  are respectively the stiffness and the damping coefficients of the spring,  $i$  is the speed multiplier ratio and  $\eta$  is the drive train efficiency.

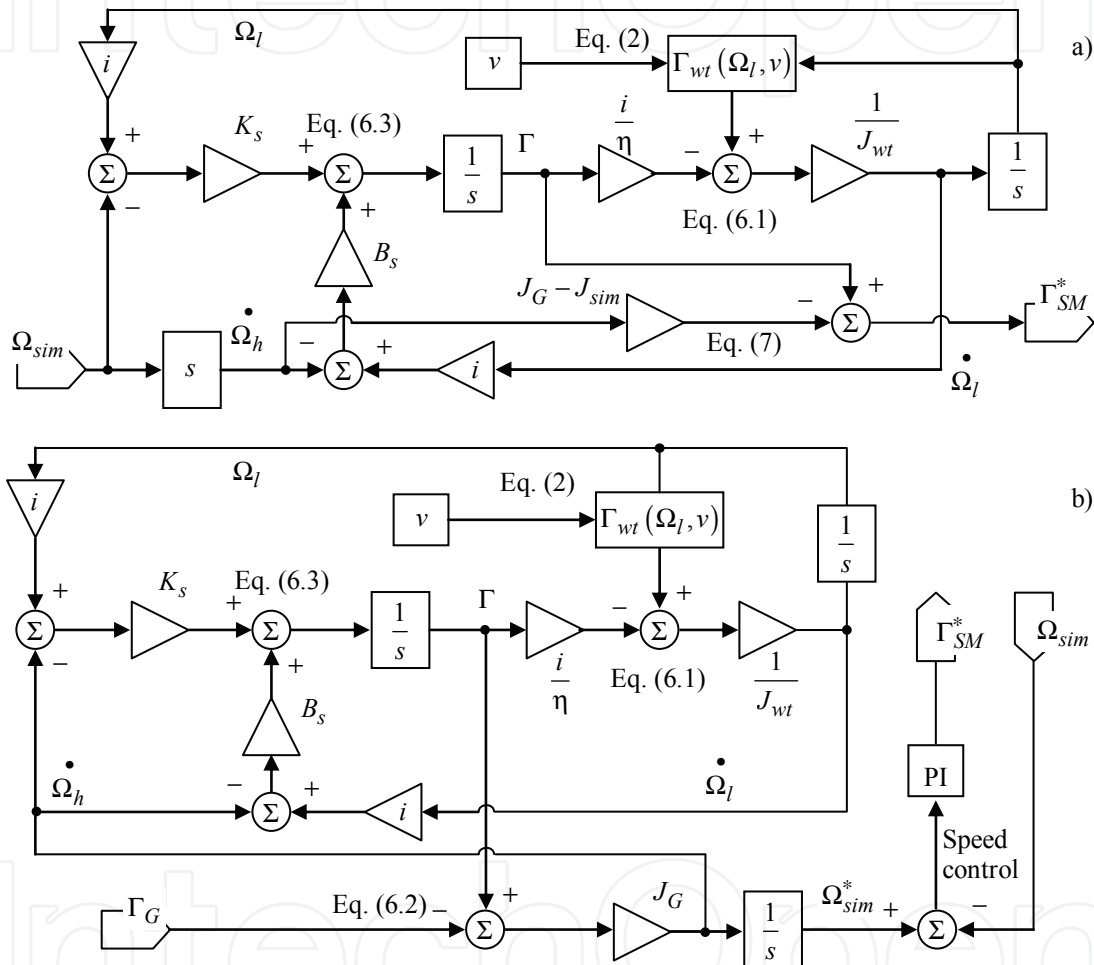


Fig. 6. RTSS configuration for WECS having flexible drive train: a) torque-driven case, b) speed-driven case

In the torque-driven case, the servomotor's torque reference is obtained based on measuring both the servomotor's rotational speed and its gradient, *i.e.*,  $\Omega_h$  and  $\dot{\Omega}_h$ , supposing that the servomotor-generator assembly emulates perfectly the high-speed shaft, *i.e.*,  $\Omega_{sim} \equiv \Omega_h$  and  $\dot{\Omega}_{sim} \equiv \dot{\Omega}_h$ . By subtracting the second equation of (6) from equation (4) one obtains:

$$\Gamma_{SM}^* = \Gamma - (J_G - J_{sim}) \cdot \dot{\Omega}_h, \quad (7)$$

where  $\Gamma$  is obtained by integrating the first and the third equation of system (6). Like in the rigid drive train case, equation (7) shows that the torque value imposed to the servomotor is

the difference between the internal torque and the dynamical torque, computed by estimating the simulator's rotational speed gradient. The corresponding block diagram to implement in the RTSS is given in Figure 6a).

In the speed-driven case, the servomotor's rotational speed reference is obtained by integrating the system of equations (6). A measure of the generator torque,  $\Gamma_G$ , should be available. The block diagram to implement, in the case when the simulator speed controller is also embedded into the RTSS, is shown in Figure 6b).

### 2.5 Which elements to employ?

The simulator is centred on the electromechanical assembly. This is made up by rigidly coupling similarly-sized servomotor and electrical generator (in power and speed) – element 1 in Figure 7. The generator has the same type as in the real WECS and determines the configuration of the power circuit ensuring the electrical power transfer to the grid/load – elements 2 and 3 in Figure 7. Corresponding to the power circuit structure one may employ a control circuit or digital system dedicated to the power flow control. Various measuring devices such as encoders, current and voltage transducers, and some other power elements, such as insulation transformers or circuit breakers are likely to be used (*e.g.*, item 4 in Figure 7). All these elements, composing and controlling the power generation system, form together what is called in the general HIL simulation methodology as the IPS. For example, if the WECS is squirrel-cage induction generator-based, a back-to-back power electronics converter must be used, if it is about a permanent-magnet synchronous generator (PMSG), the power circuit may include a diode rectifier, DC-DC and DC/AC converters, and so on.

In order to control the servomotor torque, a power electronics device – depending on the servomotor type – must be employed (*e.g.*, item 5 in Figure 7). The servomotor voltages, currents and rotational speed must be supervised; therefore the associated transducers must be present in the so-called effector. For example, if the servomotor is a DC machine, a full-bridge chopper should be used for driving purposes. Using this hardware, a current loop can be built using classical control algorithms implemented on a digital signal processor.

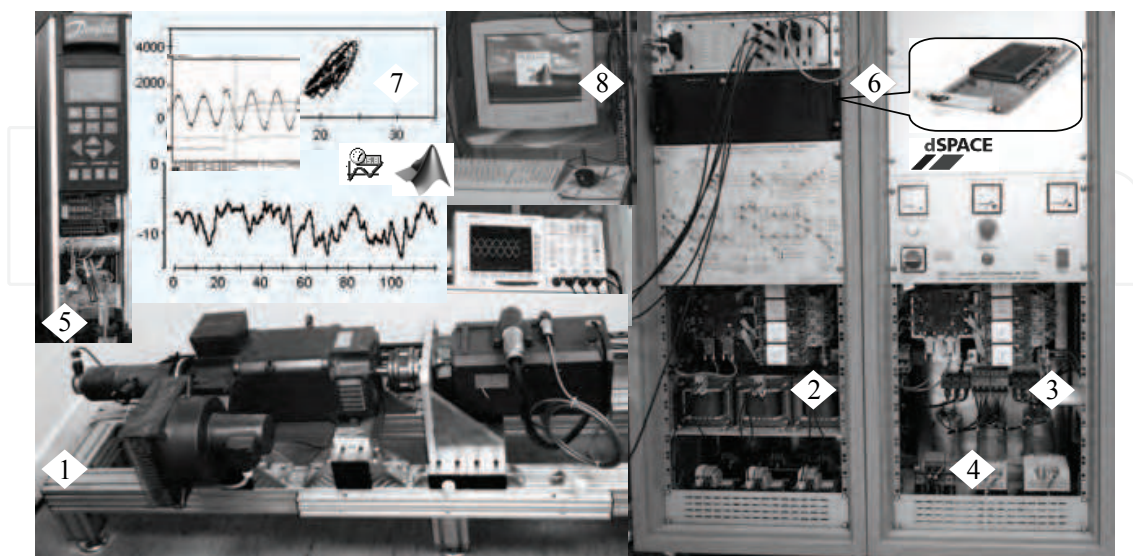


Fig. 7. Components of the WECS simulator: 1 – electromechanical assembly; 2, 3 – back-to-back power electronics converter; 4 – generic power elements; 5 – servomotor drive; 6 – digital system; 7 – user interface; 8 – host computer

According to Section 2.2, the plant to be simulated, EPS, must be translated into an algorithm, RTSS. Additionally, this latter contains wind speed models, electrical generator torque estimation, measures (inputs) filtering and output conditioning modules and should be implemented into a sufficiently fast digital system (element 6 in Figure 7). One must note that its computing step time (hundreds of microseconds in this case) is critical to the physical simulator performances. Beside this, the software-hardware loop overall lag contains some delays due to transducers, anti-aliasing filters and I/O system. Most of the applications encountered in the literature are supported by advanced, fast and flexible digital systems allowing rapid prototyping and changing of the software simulator. The dSPACE (*e.g.*, DS 1103 PPC) (Teodorescu & Blaabjerg, 2004), RTDS (RTDS, 2009) or RT-LAB (RT-LAB, 2009) systems are among these. Frequently, one uses the same systems for implementing the IPS-related control algorithms, also. Multiple interfaces (generically represented by element 7 in Figure 7) allowing the building of the software applications and the supervision of the WECS simulator may be used in conjunction with these digital systems. Element 8 in Figure 7 represents the host computer that supports these interfaces.

## 2.6 Is the WECS simulator well-performing enough? Errors analysis

A WECS real-time simulator is a laboratory tool very useful for applicative research envisaging control subsystem design or grid interfacing. In this context, the assessment of the simulator performance and the analysis of the simulation errors must be performed before the simulator is effectively used (Diop et al., 2000). Accumulation of errors begins in the modelling phase. Ideally, a physical simulator implements the adopted model, this is why the physical system modelling must correspond to the goal of simulator-based experiments. As regards the simulation errors, they can be minimized if properly configuring the real-time computing system. Unlike these two kinds of errors, it is not obvious how to minimize the tracking errors due to real-world implementation, as they depend on the way of choosing the driving variable. In the following, these latter errors in WECS simulators are analysed in the frequency domain, based on the linearized model of wind turbine (Munteanu et al., 2008a).

The linearized models of a wind turbine around a conveniently chosen steady-state operating point can be seen in Figure 8, where the influence of the two exogenous signals – the wind speed as a perturbation and the electromagnetic torque as a control input – on the plant's output have been represented. The plant's output is the high-speed rotational speed, provided that, for sake of simplicity, the case of a rigid drive train is considered. Notation  $\Delta \bullet$  denotes variations of the variable around the point of linearization. The transfer from the wind speed to the high-speed shaft rotational speed can be identified in Figure 8a), whereas the transfer from the electromagnetic torque to the same rotational speed is shown in Figure 8b). The two transfer functions will be denoted by  $H_{wt}^v$  and  $H_{wt}^{\Gamma_G}$  respectively.

In Figure 8 the following coefficients have been introduced:

$$K_{\Gamma_v} = \frac{\overline{\partial \Gamma_{wt}}}{\partial v}, \quad K_{\Gamma_\Omega} = \frac{\overline{\partial \Gamma_{wt}}}{\partial \Omega_h}, \quad (8)$$

where notation  $\overline{\bullet}$  denotes the value in the steady-state point of linearization. In Figure 8a) is considered that the rotational speed variations should be reflected in a change of the control input,  $\Gamma_G$ . This influence is modelled by means of a transfer function denoted by

$H_l(s)$ , therefore the only input of the system is the perturbation,  $\Delta v$ . Simple calculations allow obtaining the transfer function of the channel wind speed to rotational speed as:

$$H_{wt}^v(s) = \frac{\Delta\Omega_h(s)}{\Delta v(s)} = \frac{K_{\Gamma v}}{H_l(s) + J_h s - K_{\Gamma\Omega}} \quad (9)$$

The same applies for the block diagram in Figure 8b), where the influence of the perturbation has been cancelled in order to allow the electromagnetic torque to rotational speed transfer being mathematically described as:

$$H_{wt}^{\Gamma_G}(s) = \frac{\Delta\Omega_h(s)}{\Delta\Gamma_G(s)} = -\frac{1}{J_h s - K_{\Gamma\Omega}} \quad (10)$$

The accuracy of the real-time simulation is judged in relation to the capacity of the simulator to replicate the original WECS's behaviour on both transfer channels from the exogenous inputs to the system's output. In the following, the linearized models of the real-time simulation diagrams for both the torque-driven case and the speed-driven case are deduced, in order to be compared to relations (9) and (10). In this context, one can develop an errors analysis and emphasize the conditions in which these errors are minimized.

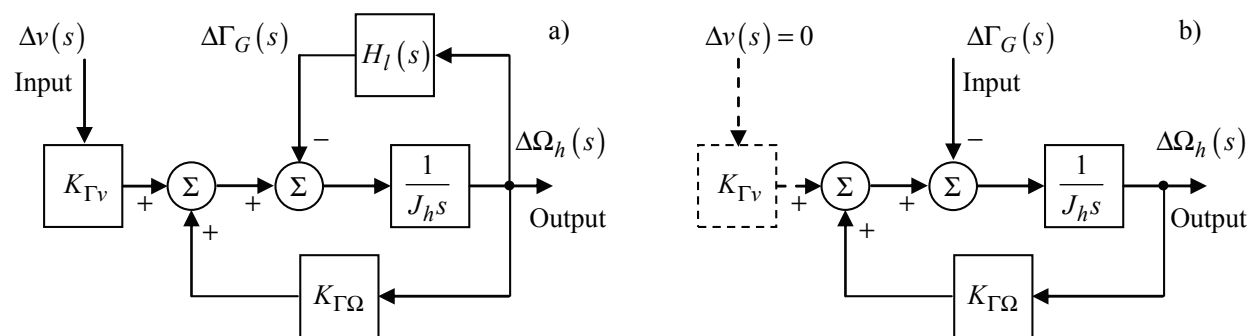


Fig. 8. Linearized model of the wind turbine: a) wind speed to rotational speed transfer; b) electromagnetic torque to rotational speed transfer

Figure 9 presents the linearized models of the real-time simulation diagram in the torque-driven case for both input-output channels, *i.e.*, from the wind speed to the simulator's rotational speed (Figure 9a) and from the electromagnetic torque to the simulator's rotational speed (Figure 9b). The two transfer functions will be denoted by  $H_{td}^v$  and  $H_{td}^{\Gamma_G}$  respectively.  $H_0^\Gamma$  is the transfer function of the servomotor torque realization. Some simple algebra allows obtaining the transfer functions of the two influence channels in the torque-driven case as follows:

$$H_{td}^v(s) = \frac{\Delta\Omega_{sim}(s)}{\Delta v(s)} = \frac{K_{\Gamma v} \cdot H_0^\Gamma(s)}{J_{sim} s + H_l(s) + H_0^\Gamma(s)((J_h - J_{sim})s - K_{\Gamma\Omega})} \quad (11)$$

$$H_{td}^{\Gamma_G}(s) = \frac{\Delta\Omega_{sim}(s)}{\Delta\Gamma_G(s)} = \frac{1}{J_{sim} s + H_0^\Gamma(s)((J_h - J_{sim})s - K_{\Gamma\Omega})} \quad (12)$$

A good quality of the real-time replication is obtained when the simulator's transfer functions  $H_{td}^v$  and  $H_{td}^{\Gamma_G}$  approach the analogous genuine WECS's transfer functions,  $H_{wt}^v$



and  $H_{wt}^{\Gamma_G}$  respectively. This reflects the replication of the WECS rotational speed,  $\Omega_h$ , by the simulator's rotational speed,  $\Omega_{sim}$ . By comparing relations (9) and (11), respectively (10) and (12), one can remark that it is sufficient that the transfer function  $H_0^\Gamma$  to approach 1 in order to have both  $H_{td}^v \rightarrow H_{wt}^v$  and  $H_{td}^{\Gamma_G} \rightarrow H_{wt}^{\Gamma_G}$ , *i.e.*, good real-time replication of the WECS's input-output behaviour. The requirement  $H_0^\Gamma \rightarrow 1$  means to ensure a very fast dynamic response of the torque loop, which is realistically achievable.

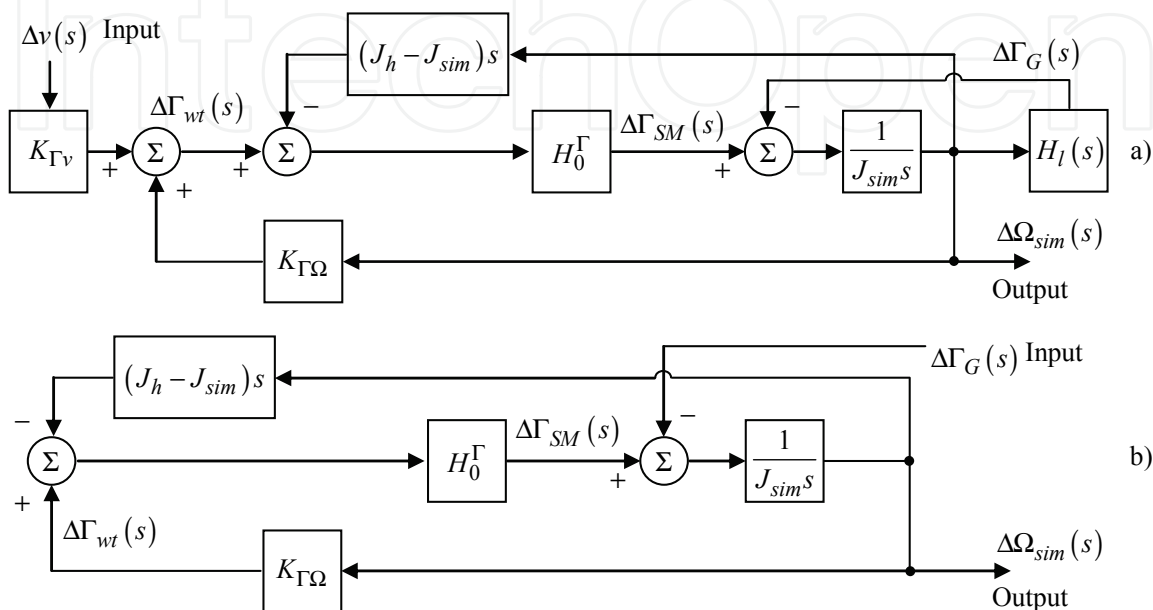


Fig. 9. Linearized model of the real-time simulation diagram in the torque-driven case: a) wind speed to simulator's rotational speed transfer; b) electromagnetic torque to simulator's rotational speed transfer

As regards the speed-driven case, one can see in Figure 10 the linearized models of the real-time simulation diagram for both input-output channels, *i.e.*, from the wind speed to the simulator's rotational speed (Figure 10a) and from the electromagnetic torque to the simulator's rotational speed (Figure 10b). The associated transfer functions will be denoted by  $H_{sd}^v$  and  $H_{sd}^{\Gamma_G}$  respectively. Notation  $R_\Omega$  corresponds to the transfer function of the rotational speed controller, whereas  $H_0^\Gamma$  keeps the meaning of transfer function of the servomotor torque realization.

Supposing that the requirement  $H_0^\Gamma \rightarrow 1$  is fulfilled, after some calculations, the transfer functions of the two influence channels in the speed-driven case result as follows:

$$H_{sd}^v(s) = \frac{\Delta \Omega_{sim}(s)}{\Delta v(s)} = \frac{K_{\Gamma v}}{\left(\frac{J_{sim}s + H_l(s)}{R_\Omega} + 1\right)(J_h s - K_{\Gamma \Omega}) + H_l(s)} \tag{13}$$

$$H_{sd}^{\Gamma_G}(s) = \frac{\Delta \Omega_{sim}(s)}{\Delta \Gamma_G(s)} = -\frac{1}{J_{sim}s + 1} \left( \frac{1}{J_h s - K_{\Gamma \Omega}} + \frac{1}{R_\Omega} \right) \tag{14}$$

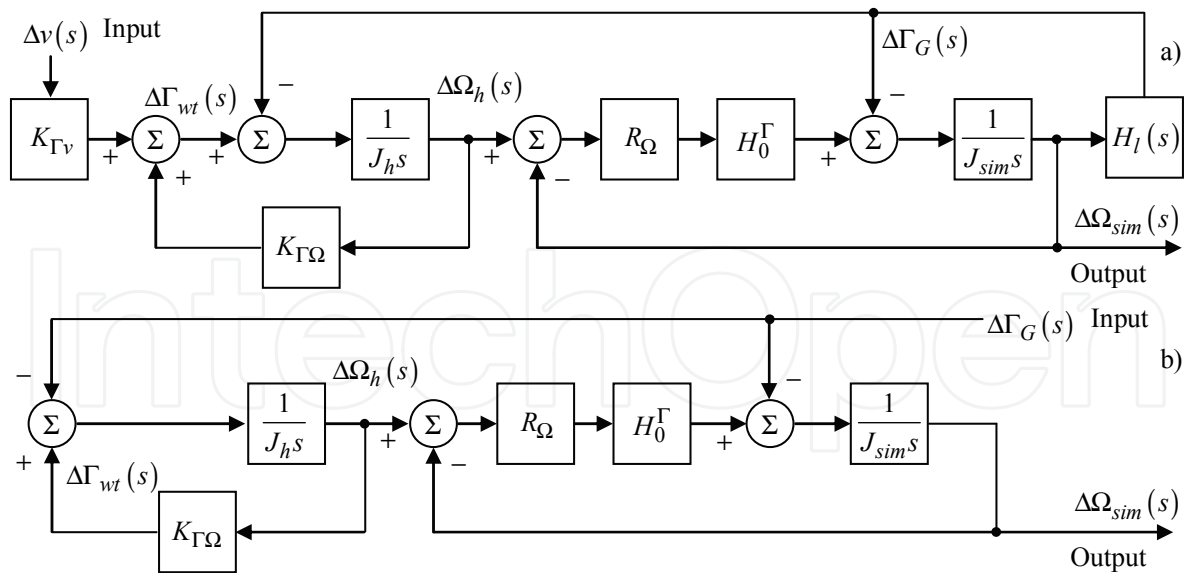


Fig. 10. Linearized model of the real-time simulation diagram in the speed-driven case: a) wind speed to simulator's rotational speed transfer; b) electromagnetic torque to simulator's rotational speed transfer

Following an inference analogous to the torque-driven case, one can remark that it is sufficient for the transfer function of the rotational speed controller to have a high gain in order to obtain a satisfactory input-output behaviour replication. Indeed, according to relations (13) and (14) compared with (9) and (10) respectively, if  $R_\Omega \rightarrow \infty$ , then both  $H_{sd}^v \rightarrow H_{wt}^v$  and  $H_{sd}^{\Gamma_G} \rightarrow H_{wt}^{\Gamma_G}$ .

Note that a similar approach can be developed for the case when the mechanical transmission consists of a flexible drive train.

As a conclusion, the simulation error is generally expressed by the difference of the rotational speeds between the WECS and the real-time simulator under the same wind velocity sequence and the same control input sequence respectively. Thus, the errors can be frequency-domain characterized by the following relation:

$$H_e^{v,\Gamma_G}(s) = H_{wt}^{v,\Gamma_G}(s) - H_{td,sd}^{v,\Gamma_G}(s), \quad (15)$$

where, in the case of a rigid drive train,  $H_{wt}^{v,\Gamma_G}(s)$  is given by relations (9) or (10) and  $H_{td,sd}^{v,\Gamma_G}(s)$  stands for one of the transfer functions in relations (11), (12), (13) or (14). In general, the error  $A_e^{v,\Gamma_G}[\text{dB}] = 20 \cdot \log(|H_e^{v,\Gamma_G}(j\omega)|)$  increases with the frequency in the EFT bandwidth, but for higher frequencies, the error is continuously decreasing due to the strictly causal nature of the system  $H_e^{v,\Gamma_G}(s)$  (Diop et al., 2000). The error in speed-driven simulators grows faster with the frequency than in the torque-driven simulator case. An improvement can be brought by the use of fast-dynamic servomotors.

A general expression of minimizing the simulation dynamic errors is by means of an integral criterion defined on a large time horizon. In this case, the minimization of the error power spectrum appears as well suited. The power spectra of the exogenous signals - wind velocity and electromagnetic torque - strongly influence the error. Figures 11 a) and b) respectively show the relative position of these spectra to the corresponding error frequency characteristic. The EFT bandwidth must be chosen such that it includes the wind velocity

spectrum and the WECS bandwidth, meanwhile ensuring small enough values of errors  $A_{\epsilon}^{v,\Gamma_G}(\omega_{\text{EFT}})$ . Consequently, two integral criteria can be defined, each of which contains the error expressed by the absolute value of the quantity in relation (15) weighted by the power spectrum of the corresponding exogenous signal (Diop et al., 2000):

$$I^{v,\Gamma_G} = \frac{1}{\pi} \cdot \int_0^{\infty} |H_{wt}^{v,\Gamma_G}(j\omega) - H_{td,sd}^{v,\Gamma_G}(j\omega)| \cdot S_{v,\Gamma_G\Gamma_G}(\omega) d\omega \quad (17)$$

The problem of simultaneously minimizing the index associated to the wind velocity and that of the electromagnetic torque is an issue under investigation.

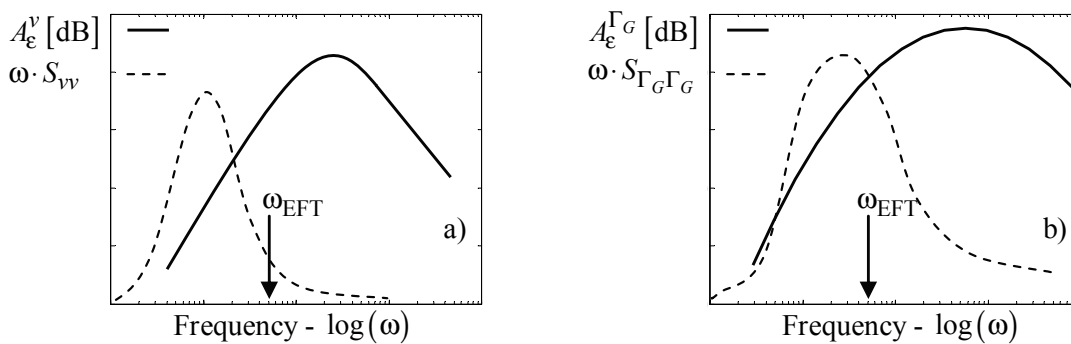


Fig. 11. Performance assessment of the simulation accuracy by frequency characterization of the model errors: a) in relation to the perturbation input (wind speed); b) in relation to the control input (electromagnetic torque)

### 3. Case study: PMSG-based WECS real-time physical simulation

The wind energy conversion topologies are various and one can note significant differences from a case to another (*e.g.*, the one using doubly-fed induction generator *vs.* the one with a PMSG). The control system structure depends in general on the particularities of the delivery point (if it is about a strong or weak grid, isolated load, *etc.*). The final scope of a WECS simulator being the testing of the control algorithms, it usually contains the necessary actuators exactly as they are in the real-world system. In this way, the IPS is fixed and the experimental rig can simulate a precisely identified class of WECS based on a given topology, whereas its software simulation capabilities are those which confer flexibility.

#### 3.1 Description of the WECS to simulate

In this case study, the approached WECS has a horizontal-axis fixed-pitch 3-bladed rotor and is connected to an infinite power grid. The rotor is placed upwind and is oriented normally on the wind by means of a vane. The mechanical transmission consists of a rigid single-step speed multiplier. The power generation structure is based on a PMSG whose stator is grid-connected by means of a back-to-back power electronics converter. The decoupling from the grid is thus achieved and the variable-speed regime is made possible. For details concerning both the aerodynamic and the electrical features of the WECS, the reader is sent to the Appendix. As Figure 12 shows, two kinds of controllers ensure the transfer of the converted power to the electrical grid. The first one implements the PMSG

torque/speed control by acting on the generator-side converter, whereas the second one acts on the grid-side converter aiming at maintaining the DC-link voltage at an imposed level. In the context of the methodology presented in the previous sections, the above described system is the original one, for which the control problem formulation is generally complex. The reason is that not only the output power must be controlled, *i.e.*, by the grid-side converter, but also the behaviour of the coupling turbine-generator. Therefore, the control objective depends on the WECS regime: in partial load one must ensure the maximisation of the power captured from the wind by using the variable-speed capability, while in full load the power limitation is mandatory (Burton et al., 2001).

The WECS modelling assumptions are related to its rated power. This case study is focused on a low-power WECS (less than ten kilowatts). Thus, as the blades length is relatively small, many effects due to rotor interaction with the wind stream or with the tower are negligible. Also, if the rotor's rotational speed is large enough *vs.* the lateral wind speed component dynamics, a scalar model can be used for the wind speed (Burton et al., 2001).

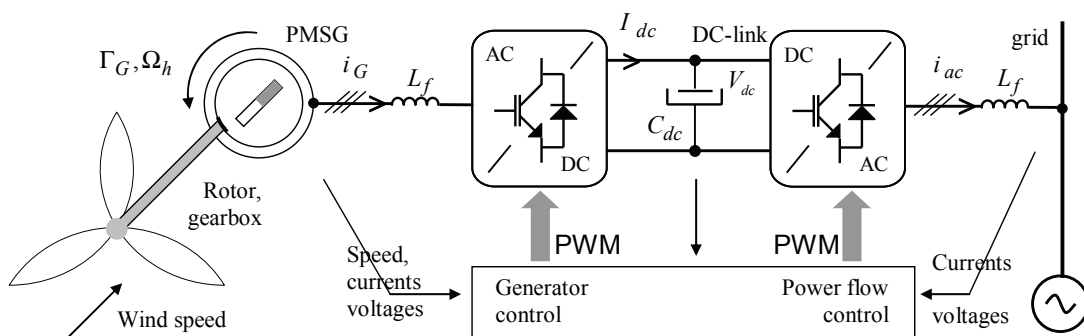


Fig. 12. Topology of the WECS to simulate

As general requirement, the simulator has to replicate the dynamic behaviour of various wind turbines belonging to the described WECS class under variable wind conditions and in different operating regimes. The rated power of the generator within the test rig is limited, therefore the simulator must offer the possibility of changing the scale factors in order to emulate wind turbines of various power sizes and also the possibility of switching between various control laws. Flexibility is also reflected by the facility of changing the parameters of the wind turbine and those of the wind site. Design of a friendly user interface enables the manipulation of the simulation parameters and experimental results.

### 3.2 Building of the RTPS

#### 3.2.1 Splitting of the original system and identification of the interaction variables

Taking account of considerations stated in §2 the interaction EPS-IPS takes place at the high-speed (electrical generator) shaft, by means of mechanical interaction variables, namely the mechanical torque and the high-speed shaft rotational speed. Consequently, the subsystem under test (IPS) contains the electrical part of the WECS, which is taken as it is from the original system, *i.e.*, the PMSG, the AC/DC/AC converter and the grid. The aerodynamic interactions and mechanical transmission behaviours must be simulated, so be included into the subsystem to be simulated (EPS). Synthetic wind velocity will be used to excite the EPS model (already detailed in §2.3), thus ensuring controllable test conditions.

### 3.2.2 Effector configuration

The information exchange between the software simulator and the IPS is possible by means of the physical part of the RTPS. In this case study the chosen driving variable is the high-speed shaft mechanical torque,  $\Gamma_R$ , therefore the response variable will be the high-speed shaft rotational speed,  $\Omega_h$ , which is measured by means of an encoder. The effector is implemented by a current-controlled permanent-magnet DC motor, rigidly coupled to the PMSG shaft, which is required to replicate the mechanical characteristics of the WECS high-speed shaft. The DC motor torque control ensures a very fast EFT dynamic. As the driving variable is a cause variable, the model implemented in the RTSS is a non-causal one. The DC motor torque,  $\Gamma_{SM}$ , is proportional with the armature current and must emulate the evolution of  $\Gamma_R$ , such that the rotational speed of the simulator,  $\Omega_{sim}$ , to replicate the real dynamical evolution of the response variable,  $\Omega_h$ . By using equations (3) and (5) one obtains the DC machine (EFT) reference torque:

$$\Gamma_{SM}^* = \eta \cdot \Gamma_{wt} / i - (J_{wt} \cdot \eta / i^2 - J_{sim}) \cdot \dot{\Omega}_{sim}, \quad (17)$$

where the wind torque,  $\Gamma_{wt}$ , results from relation (2) in which a synthesized wind speed,  $v$ , is used. Finally, the model to implement in the RTSS is composed of relations (2) and (17).

### 3.2.3 RTSS design

In Figure 13 one can remark the structure of the WECS simulator, where the IPS and the RTPS have been represented. One can note the two main components of the RTPS: the hardware part (the effector and the speed transducer) and the software part (the real-time software simulator, RTSS). Being implemented based on the MathWorks xPC Target® (MathWorks, 2008), the RTSS must perform the following tasks:

- to compute a wind speed sequence by using a pseudo-random model or a deterministic one (Nichita et al., 2002), and to read the value of the response variable,  $\Omega_h$ ,
- to implement the EPS model - relations (2) and (17) - and
- to compute the reference value of the driving variable,  $\Gamma_{SM}^*$ , which is sent to the EFT.

These are coded within a MATLAB®/Simulink® diagram; this is compiled using Real-Time Workshop and C compiler on the host PC and downloaded on the target PC via TCP/IP.

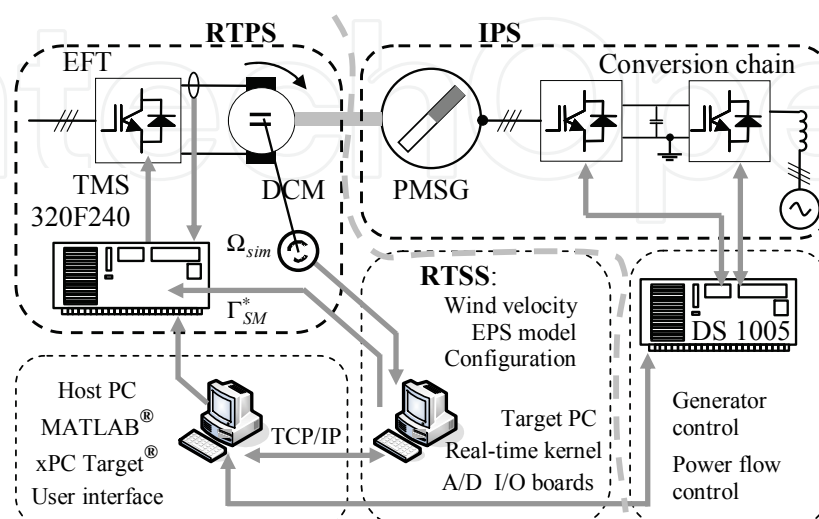


Fig. 13. RTPS and IPS identified on the schematic of the WECS simulator



Further, the target PC runs the real-time application and exchanges information with the hardware part of the RTPS by means of a PCI I/O interface (PCI-DAS1200/JR and PCIM-DDA 06/16 boards – Measurement Computing, 2008). The driving variable,  $\Gamma_{SM}$ , is implemented physically by using the DC machine, namely based upon the proportionality between the torque and the armature current. Thus, a current tracking loop is designed, whose components can be viewed in Figure 13: a current transducer, a numerical PID controller supported by a fixed-point DSP, TMS320F240, and an actuator composed of a 4-quadrant PWM IGBT chopper connected with a diode rectifier. The settling time of the DC-machine current is 4 ms, corresponding to a sufficiently fast EFT dynamic. For more details about the RTPS specification the reader is sent to the Appendix.

### 3.3 Building of the IPS

#### 3.3.1 PMSG control

In the case of grid-connected WECS, the wind turbine generator control objective is to maximize the output power in partial load and to limit it at the rated value in full load. This regime is obtained by variable-speed operation, *i.e.*, by imposing a suitable generator rotational speed reference, depending on the turbine operating regime: in partial load this reference is outputted by a MPPT algorithm, while in full load it is generally given by a power regulation controller. Thus, the power control is entirely achieved by means of the generator control. A control structure called self-controlled synchronous machine is built for the PMSG vector control (Bose, 2001). It employs an AC-DC converter and an absolute position encoder. By imposing the PMSG stator voltages, the output current and hence the machine torque is controlled by separately controlling the Park current components,  $i_{sd}$  and  $i_{sq}$ . On each  $d$  and  $q$  channels anti-windup PI controllers are used, which are tuned by the well-known modulus criterion, thus ensuring an optimal trade-off between the settling time and the overshoot of the closed-loop step response (Åström & Hägglund, 1995). The PMSG speed control relies on employing an outer loop over the  $q$  channel control loop, which is based on a PI controller – designed according to the symmetrical optimum criterion – outputting the electromagnetic torque reference, hence the  $i_{sq}$  reference value.

#### 3.3.2 Control of the power transfer to the grid

The DC-to-AC power transfer control is ensured by the grid-side converter (see Figure 12). The plant is composed of a DC-link bus, a DC-AC converter and the electrical grid. The 3-phased currents are fed into the mains while controlling the DC-link voltage at a constant value. If the considered WECS is part of a wind farm, of high impedance, it must also be able to supply reactive power to the grid in order to compensate voltage variations at the point of common coupling. Two current control loops are built for the  $q$  and  $d$  Park components respectively; an outer voltage control loop is in charge with regulating the DC-link voltage,  $V_{dc}$ , at an imposed value (Gombert et al., 2006). The DC-link voltage controller provides the  $i_{acq}^*$  reference, while a nonzero value of  $i_{acd}^*$  corresponds to reactive power to be supplied to the grid. The inner loops output the grid voltage references in the  $(d,q)$  frame, which are further transformed into a 3-phased system and applied to the inverter. These loops are all based upon anti-windup PI controllers which are tuned according to the modulus optimum criterion. A software 3-phased phase-locked loop is used in order to provide the grid electrical angle (Kaura & Blasko, 1997; Rabelo & Hofmann, 2002).

### 3.3.3 Hardware and software support of the control loops within the IPS

The control loops described above are supported by some widely-used hardware: three-leg IGBT power converters and associated gate drivers, current and voltage sensors, LC filters, incremental encoder and electrical connection equipment (Figure 12). As regards the software component of the control loops, this is supported by a dSPACE modular hardware around the DS 1005 PPC board (dSPACE, 2008), whose I/O system allows information being exchanged in both logic and analogic form. The program on DS 1005 runs two tasks:

- a *main (interruption) task*, with the highest priority, in charge with real-time operations;
- a *background task*, which updates the DSP memory by means of an user interface.

Simulation diagrams implementing the two tasks have been built in MATLAB®/Simulink® on the dSPACE host PC computer, then transferred to the target processor by using the Real Time Workshop and C compiler. The diagrams allow the main parameters being modified on-line. A ControlDesk® panel and an oscilloscope allow visualizing the interest variables.

### 3.4 Errors analysis

Figure 14 displays information about the accuracy of the simulation results provided by the real-time simulator and allows the stability of the simulation being assessed. Thus, the simulation errors are evaluated over a sufficiently large frequency domain (three decades), which must include the spectra of the exogenous signals, according to the method presented in §2.6. The measured frequency response in rotational speed of the real-time simulator is compared with its “should-be” value, *i.e.*, that of the model, with respect to both exogenous signals, the wind speed (frequency-bounded stochastic disturbance) and the electromagnetic torque (control input). Variable-frequency sinusoidal variations of the exogenous signals around a typical steady-state point were applied to the simulator in order to obtain its frequency response. An operating point in the vicinity of the maximum power point was chosen, which corresponds to an average wind speed of 8 m/s, electromagnetic torque -5.4 N·m and rotational speed 245 rad/s. For sake of correctness, the model of the rotational speed transducer effectively used on the test rig has been included in the WECS model.

By analyzing the simulator’s frequency response with respect to the wind speed, along with a typical spectral density of the wind turbulence – exhibiting most of energy between 0.1 and 1 rad/s (Burton et al., 2001) – one can remark that the simulation errors are reasonably small for almost the whole frequency range considered, which totally includes the wind speed spectrum (Figure 14a). Therefore, the simulator replicates almost exactly the original system subject to the wind speed variations.

The same type of results has been obtained with respect to the electromagnetic torque – see Figure 14b). In this case the amplitude errors are larger, but however almost constant (3 dB) over the whole frequency range of interest, therefore easy to compensate by control action if needed. The electromagnetic torque has a controllable dynamic, essentially following the dynamic of the main disturbance, *i.e.*, of the wind turbulence, except the high-frequency variations for reasons of minimizing the fatigue loads (Burton et al., 2001). The error evaluation is therefore relevant in almost the same frequency range as in the case of wind turbulence. Both sets of results exhibit increases of the error at high frequency, but this is not critical as the disturbances have low content of high-frequency spectra.

Concerning the stability of the real-time simulation schemes implemented, it can be verified if the emulation dynamic is sufficiently fast with respect to the dynamics to be emulated. The emulation dynamic is expressed by the settling time of the effector. In this case study,

the effector responds in about 4 ms, in other words, it has a bandwidth of about 1000 rad/s, which largely includes the dynamics to be emulated (Figure 14). In conclusion, the delays introduced by the emulation in the frequency range of interest can reasonably be neglected.

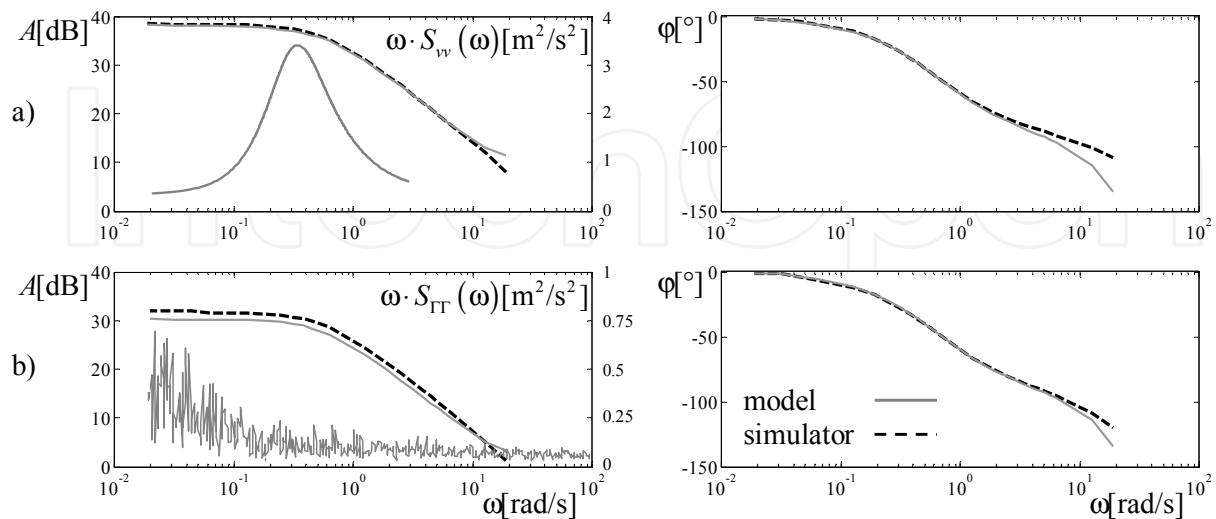


Fig. 14. Measured frequency responses – amplitude and phase lag – of the simulator in comparison with those of the WECS model: a) wind velocity to rotational speed transfer, b) electromagnetic torque to rotational speed transfer

### 3.5 Performance evaluation

#### 3.5.1 Replication of the main operating regimes: partial load and full load

In the partial-load regime – which is in this case study delimited by the rated wind speed 11 m/s – the output power depends proportionally on the wind velocity cubed and the rotational speed varies proportionally with the wind velocity, whereas the aerodynamic efficiency is at its maximum value. The full-load regime is characterized by the wind velocity going beyond the rated value. In this regime, the rotational speed is adjusted such that to limit the output power at rated; meanwhile, the power coefficient significantly decreases with the wind speed. Figure 15 presents the replication of the steady-state characteristics of the studied WECS, where the two main operating regimes are identified.

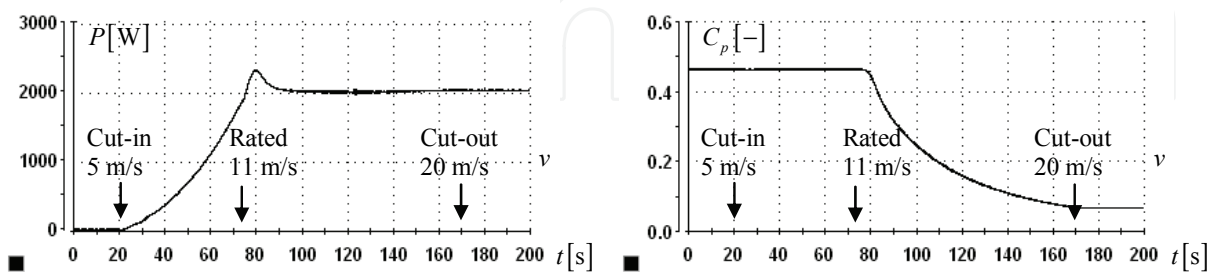


Fig. 15. WECS steady-state characteristics, as replicated by the real-time simulator: a) provided power *vs.* wind speed; b) power coefficient *vs.* wind speed

The two regimes are respectively managed by two PI controllers providing the rotational speed references. The aim of the partial-load controller is to maintain the power coefficient at its maximum value based on the wind velocity and rotational speed measures. At the

rated wind velocity, the control is switched to the full-load controller, which aims at regulating the WECS output power at its rated value by changing the rotational speed in response to the measured active power fed to the grid. The reader should note that these are not the only control designs that can be envisaged for a WECS (Munteanu et al., 2008a).

Figure 16 shows how the real-time simulator replicates the WECS partial-load operation when the average wind speed is around 8 m/s. The oscilloscope captures show: a) variable-speed operation under variable wind velocity with medium turbulence intensity of  $I=0.15$ , obtained by using the von Karman spectrum in the IEC standard (Nichita et al., 2002); b) behaviour at trapeze-shaped wind gusts under variable-speed operation. Figure 16a) shows that the active power supplied to the grid – negative by convention – depends obviously on the wind velocity. In variable-speed operation the wind torque contains dynamic elements due to the rotational speed variations (Figure 16b), whereas the wind velocity variations are compensated such that  $\lambda$  and  $C_p$  are maintained around their optimal values.

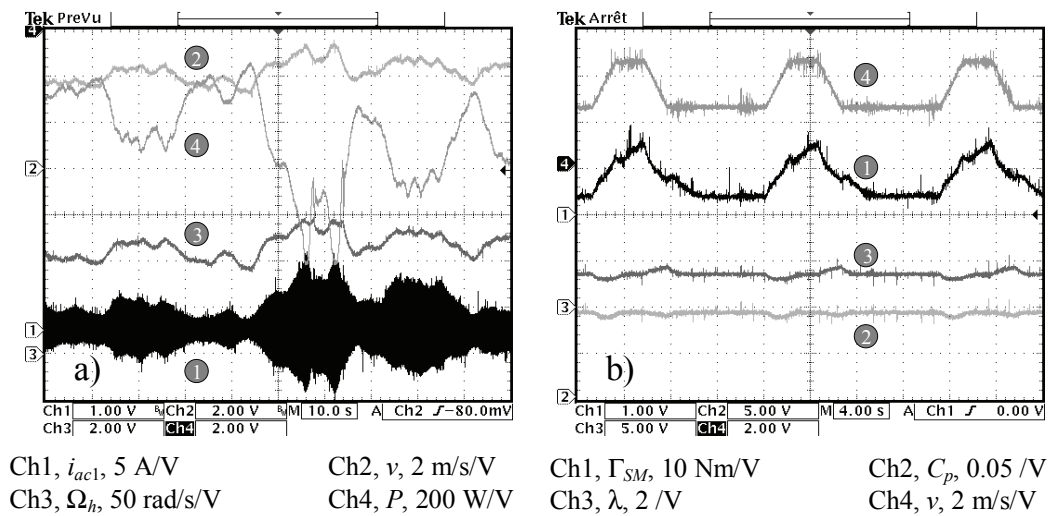


Fig. 16. Real-time replication of the WECS partial-load operation: a) under variable wind speed sequence; b) under trapeze-shaped wind gusts

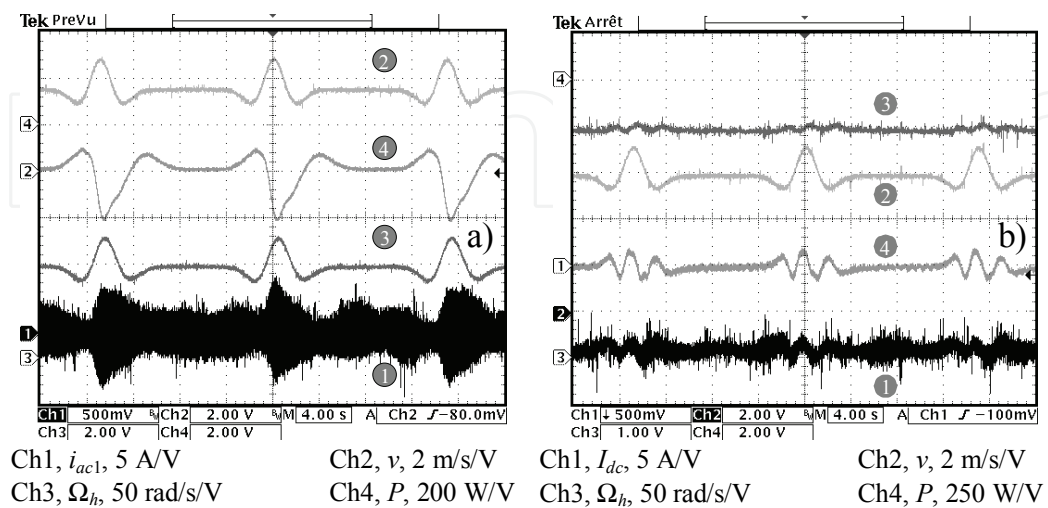


Fig. 17. Real-time replication of the WECS operation under extreme-operating wind gusts: a) in partial load; b) in full load

Globally speaking, the real-time simulations show realistic performance under both turbulent wind and extreme-operating gusts.

Figure 17 contains results concerning the real-time simulation of the WECS behaviour at bell-shaped, *i.e.*, extreme-operating, wind gusts (Burton et al., 2001), under variable-speed operation in partial-load (Figure 17a) and in full-load regime respectively (Figure 17b). The full-load controller acts on the rotational speed,  $\Omega_{ht}$ , aiming at limiting the active power at its rated value. Thus, when the wind velocity increases,  $\Omega_{ht}$  is decreased in order to reduce the power coefficient as the turbine rotor enters in deeper stall. The output power, the DC-link power and the mean value of  $I_{dc}$  are kept constant irrespective of the wind variations.

### 3.5.2 Grid power transfer

The results presented above have been obtained when reactive power generation is not required, *i.e.*, the reactive power reference is zero. The evolution of the main variables involved in the real-time simulation of the WECS-grid interaction when imposing a nonzero level of reactive power can be seen in Figures 18 and 19.

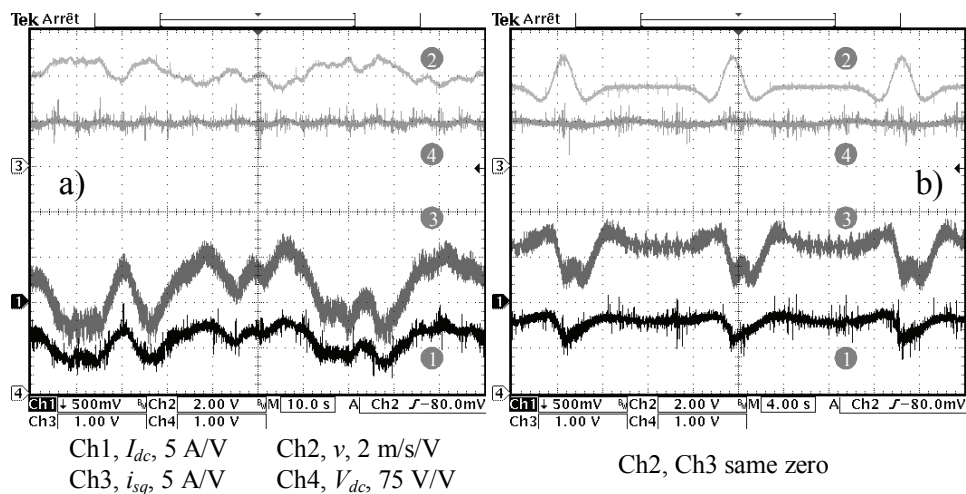


Fig. 18. RTPS – power grid interaction: a) under variable wind speed; b) under wind gusts

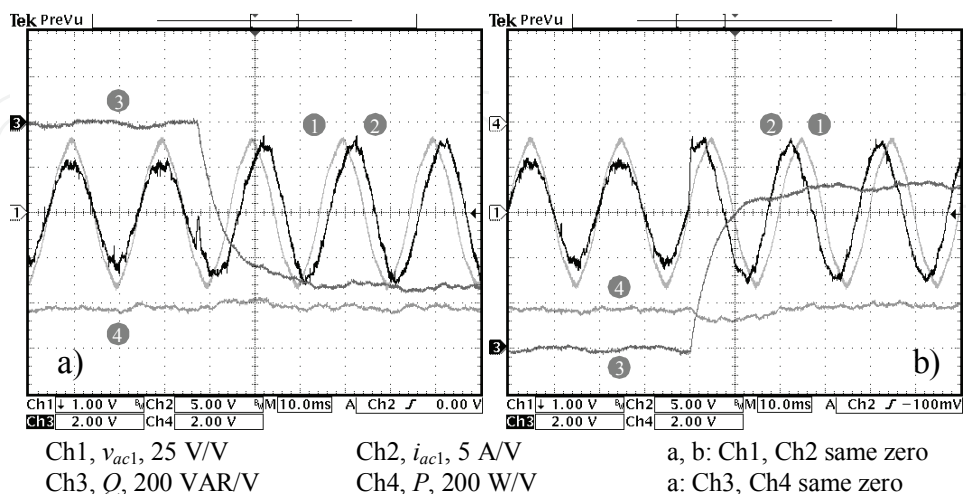


Fig. 19. RTPS – power grid interaction: a) reactive power injection into the grid; b) reactive power absorption from the grid



Results presented in Figures 18 a) and b) correspond to conditions of variable wind speed and gusts of wind speed respectively. The DC-link current,  $I_{dc}$ , varies with the wind, as the active power variation follows the wind speed variation and the DC-link voltage is maintained almost constant. The variations of the  $q$ -component of the PMSG stator current are proportional with the electromagnetic torque. Figures 19 a) and b) display the behaviour of the grid electrical variables at the point of coupling,  $v_{ac1}$  and  $i_{ac1}$ , in both cases, of reactive power injection into and, respectively, absorption from the grid. The phase lag between voltage and current is modified accordingly. The reactive power amount corresponds to imposing a nonzero reference of  $i_{acd}$ , yielding a larger value of  $i_{ac1}$ .

#### 4. Conclusion

This chapter has presented the essentials concerning the building of WECS physical simulators. It has tried to give answer to some basic practical questions. First, why using and how to build WECS simulators. Then, which elements to employ in their construction and how close can behave a physical simulator with respect to the original WECS. Last but not least, an example embedding a complete generation chain has been approached, for a better orientation of the reader throughout the complex challenge which is the WECS physical simulator building. The replication of wind turbines behaviour in a laboratory-controlled environment is done by closed-loop connecting hardware and software components in a hardware-in-the loop structure. The management of the digital system and the control of the electromechanical components are key issues in obtaining good simulator performances. In short, this complex system is built in order to replicate the turbine rotor behaviour, while subjected to controllable wind velocities, whereas the electrical conversion chain remains exactly as it is (at a certain scale) in the real wind power system.

Even if the subject has been extensively approached in the literature, it has not been depleted yet of scientific interest. In this context, an in-depth simulation errors analysis may uncover interesting theoretical results. As concerns the practical aspects, the connection of such device with a physically-simulated microgrid (Gaztañaga et al., 2007) may boost its capabilities and enlarge its range of applications.

#### 5. Appendix

List of acronyms

EFT	effector
EPS	emulated physical system
HAWT	horizontal-axis wind turbine
IPS	investigated physical system
(P)HIL	(power) hardware-in-the-loop
PMSG	permanent-magnet synchronous generator
RTPS	real-time physical simulator
RTSS	real-time software simulator
WECS	wind energy conversion system

WECS characteristics in the case study

- *aerodynamic features*: fixed-pitch 3-bladed HAWT turbine, rated output power 2 kW at  $v=11$  m/s, cut-in wind speed 5 m/s,  $R=1.7$  m,  $J_{wt}=1.5$  kg·m<sup>2</sup>, maximal power coefficient  $C_{p_{max}}=0.47$  at optimal tip speed ratio  $\lambda_{opt}=7.4$ , 6.5x rigid drive train;

- *electrical components*: PMSG Siemens 1FT6084-8SK71-1TGO, rated values of: power – 6 kW, speed – 3000 rpm, torque – 22 Nm, voltage – 135 V; inertia 0.0048 kg·m<sup>2</sup>, 4 poles,  $R_s = 173.77 \text{ m}\Omega$ ,  $L_{sd} = 0.8524 \text{ mH}$ ,  $L_{sq} = 0.9515 \text{ mH}$ ,  $\Phi_f = 0.1112 \text{ Wb}$ ; IGBT Semikron SKM 50 GB 123D-based three-leg voltage source inverters, 5 kW, 10 kHz; Semikron SKHII22A gate drivers; DC-link  $V_{dc} = 450 \text{ V}$ ,  $C_{dc} = 2200 \mu\text{F}/800\text{V}$ ;  $V_{ac} = 127/230 \text{ V} - 50\text{Hz}$ ,  $L_f = 350 \mu\text{H}/5\text{A}$ .
- *RTPS features*: 1:1 simulator, DC machine Siemens 1G 5 106-0EH-3UV1, rated values of: power – 6.4 kW, speed – 3470 rpm, torque – 20.2 Nm, voltage – 310 V; inertia 0.02 kg·m<sup>2</sup>, torque constant 0.87 Nm/A, electromechanical time constant 4.6 ms; 10 kW 3-phased bridge diode rectifier, 4-quadrant 5 kW chopper based on IGBT Semikron SKM 50 GB 123D; incremental optical encoder 1024 lines; sampling time  $T_s = 100 \mu\text{s}$ .

## 6. References

- Akhmatov, V. (2003). *Analysis of dynamic behaviour of electric power systems with large amount of wind power*, Ph.D. Thesis, Technical University of Denmark, ISBN 87-91184-18-5, Denmark
- Akhmatov, V.; Knudsen, H. & Nielsen, A.H. (2000). Advanced simulation of windmills in the electric power supply. *International Journal of Electrical Power and Energy Systems*, 22, 6, 421-434, ISSN 0142-0615
- Andreica, M.; Bacha, S., Roye, D., Munteanu, I., Bratcu, A.I. & Guiraud, J. (2009). Stand-alone Operation of Cross-flow Water Turbines. *Proceedings of IEEE International Conference on Industrial Technology – ICIT 2009*, pp. 463-468, ISBN 978-1-4244-3507-4, Churchill, Victoria, Australia, February 10-13 2009, IEEE Press
- Åström, K.J. & Hägglund, T. (1995). *PID controllers: theory, design and tuning*, 2nd edn., Instrument Society of America, ISBN 978-1556175169, U.S.A.
- Battaioto, P.E.; Mantz, R.J. & Puleston, P.F. (1996). A wind turbine emulator based on a dual DSP processor system. *Control Engineering Practice*, 4, 9, 1261-1266, ISSN 0967-0661
- Bose, B.K. (2001). *Modern power electronics and AC drives*, Prentice-Hall, ISBN 978-0130167439, Englewood Cliffs, NJ, U.S.A.
- Burton, T.; Sharpe, D., Jenkins, N. & Bossanyi, E. (2001). *Wind energy handbook*, John Wiley & Sons, ISBN 978-0471489979, New-York
- Camblong, H.; Martinez de Alegria, I., Rodriguez, M. & Abad, G. (2006). Experimental evaluation of wind turbines maximum power point tracking controllers. *Energy Conversion and Management*, 47, 18-19, 2846-2858, ISSN 0196-8904
- Cárdenas, R.; Asher, G.M., Ray, W.F. & Peña, R. (1996). Power limitation in variable speed wind turbines with fixed pitch angle. *Proceedings of International Conference on Opportunities and Advances in International Electric Power Generation*, pp. 44-48, ISBN 0-85296-655-5, Durham, U.K., March 18-20, IEE, London
- Cárdenas, R.; Peña, R., Asher, G.M. & Clare, J.C. (2001). Experimental emulation of wind turbines and flywheels for wind energy applications. *Proceedings of 9th European Conference on Power Electronics and Applications – EPE 2001*, (CD-ROM), ISBN 90-75815-06-9, Graz, Austria

- Diop, A.D.; Nichita, C., Belhache, J.J., Dakyo, B. & Ceangă, E. (1999). Modelling variable pitch HAWT characteristics for a real time wind turbine simulator. *Wind Engineering*, 23, 4, 225-243, ISSN 1991-8763
- Diop, A.D.; Nichita, C., Belhache, J.J., Dakyo, B. & Ceangă, E. (2000). Error evaluation for models of real time wind turbine simulators. *Wind Engineering*, 24, 3, 203-221, ISSN 1991-8763
- dSPACE (2008). *DS 1005 PPC Board Manual*. Available: [http://www.dspace.de/ww/en/inc/home/products/hw/modular\\_hardware\\_introduction/processor\\_boards/ds1005.cfm](http://www.dspace.de/ww/en/inc/home/products/hw/modular_hardware_introduction/processor_boards/ds1005.cfm), October 2009
- Enslin, J.H.R. & van Wyk, D. (1992). A study of a wind power converter with micro-computer based maximal power control utilizing an over-synchronous electronic Scherbius cascade. *Renewable Energy*, 2, 6, 551-562, ISSN 0960-1481
- Gaztañaga, H.; Etxeberria-Otadui, I., Ocnăşu, D. & Bacha, S. (2007). Real-Time Analysis of the Transient Response Improvement of Fixed-Speed Wind Farms by Using a Reduced-Scale STATCOM Prototype. *IEEE Transactions on Power Systems*, 22, 2, 658-666, ISSN 0885-8950
- Gombert, C.; Ocnăşu, D., Bacha, S., Roye, D. & Besanger, Y. (2006). Test of a PWM controller using a Real-Time Digital Simulator. *International Review of Electrical Engineering*, CD-ROM ISSN 1827- 6679
- Hanselmann, H. (1996). Hardware-in-the-loop simulation testing and its integration into a CACSD toolset. *Proceedings of the 1996 IEEE International Symposium on Computer-Aided Control System Design*, pp. 152-156, ISBN 0-7803-3032-3, Dearborn, MI, U.S.A., September 15-18 1996, IEEE Press
- Kaura, V. & Blasko, V. (1997). Operation of a phase locked loop system under distorted utility conditions. *IEEE Transactions on Industry Applications*, 33, 1, 58-63, ISSN 0093-9994
- Leithead, W.E.; Rogers, M.C.M., Connor, B., Pierik, J.T.E., Van Engelen, T.G. & O'Reilly, J. (1994). Design of a controller for a test-rig for a variable speed wind turbine. *Proceedings of the 3rd IEEE Conference on Control Applications*, vol. 1, pp. 239-244, ISBN 0-7803-1872-2, Glasgow, U.K., August 24-26 1994, IEEE Press
- Mathworks (2008). *xPC Target User's Guide*. Available: [www.mathworks.com/support/product/XP/productnews/xpc\\_target\\_ug\\_Nov\\_07\\_2003.pdf](http://www.mathworks.com/support/product/XP/productnews/xpc_target_ug_Nov_07_2003.pdf), October 2009
- Measurement Computing (2008). *I/O Boards Manual*. Available: <http://www.measurementcomputing.com>, October 2009
- Munteanu, I. (2006). *Contributions to the optimal control of wind energy conversion systems*, Ph.D. Thesis, "Dunărea de Jos" University of Galaţi, Romania
- Munteanu, I.; Bratcu, A. I., Cutululis, N. A. & Ceangă, E. (2008a). *Optimal Control of Wind Energy Systems – Towards a Global Approach*. Springer-Verlag, ISBN 978-1-84800-079-7, London
- Munteanu, I.; Cutululis, N.A., Bratcu, A.I. & Ceangă, E. (2005). Optimization of variable speed wind power systems based on a LQG approach. *Control Engineering Practice*, 13, 7, 903-912, ISSN 0967-0661

- Munteanu, I.; Seddik, B., Bratcu, I.A., Guiraud, J. & Roye, D. (2008b). Energy-Reliability Optimization of Wind Energy Conversion Systems by Sliding Mode Control. *IEEE Transactions on Energy Conversion*, 23, 3, 975 -985, ISSN 0885-8969
- Nichita, C.; Diop, A.D., Belhache, J.J., Dakyo, B. & Protin, L. (1998a). Control structures analysis for a real time wind system simulator. *Wind Engineering*, 22, 6, 275-286, ISSN 1991-8763
- Nichita, C.; Luca, D., Dakyo, B. & Ceangă, E. (2002). Large band simulation of the wind speed for real time wind turbine simulators. *IEEE Transactions on Energy Conversion*, 17, 4, 523-529, ISSN 0885-8969
- Rabelo, B. & Hofmann, W. (2002). DSP-based experimental rig with the doubly-fed induction generator for wind-turbines. *Proceedings of the 10th International Power Electronics and Motion Control Conference - EPE-PEMC 2002*, (CD-ROM), ISBN 953-184-046-6, Cavtat & Dubrovnik, Croatia, September 9-11 2002
- Rabelo, B.; Hofmann, W. & Gluck, M. (2004). Emulation of the static and dynamic behaviour of a wind turbine with a DC-machine drive. *Proceedings of the 35th Power Electronics Specialists Conference - PESC '04*, vol. 3, pp. 2107-2112, ISBN 0-7803-8399-0, Aachen, Germany, June 20-25 2004, IEEE Press
- Rodriguez-Amenedo, J.L.; Rodriguez-Garcia, F., Burgos, J.C., Chincilla, M., Arnalte, S. & Veganzones, C. (1998). Experimental rig to emulate wind turbines. *Proceedings of the ICEM Conference*, vol. 3, pp. 2033-2038, Istanbul, Turkey, September 2-4 1998
- RTDS (2009). *RTDS 2009 Hardware Overview*. RTDS Technologies Inc. Available: <http://www.rtds.com/hardware.htm>, October 2009
- RT-LAB (2009). Available: <http://www.opal-rt.com/product/rt-lab-professional>, October 2009
- Steurer, M.; Li, H., Woodruff, S., Shi, K. & Zhang, D. (2004). Development of a unified design, test, and research platform for wind energy systems based on hardware-in-the-loop real time simulation. *Proceedings of the 35th Annual IEEE Power Electronics Specialists Conference*, pp. 3604-3608, ISBN 0-7803-8399-0, Aachen, Germany, June 20-25 2004, IEEE Press
- Teodorescu, R. & Blaabjerg, F. (2004). Flexible control of small wind turbines with grid failure detection operating in stand alone and grid connected mode. *IEEE Transactions on Power Electronics*, 19, 5, 1323-1332, ISSN 0885-8993
- Wilkie, J.; Leithead, W.E. & Anderson, C. (1990). Modelling of wind turbines by simple models. *Wind Engineering*, 14, 4, 247-274, ISSN 1991-8763
- Wu, X.; Lentijo, S. & Monti, A. (2004). A novel interface for power-hardware-in-the-loop simulation. *Proceedings of the IEEE Workshop on Computers in Power Electronics*, pp. 178-182, ISBN 0-7803-8502-0, Urbana, Illinois, 15-18 August 2004, IEEE Press



## **Wind Power**

Edited by S M Muyeen

ISBN 978-953-7619-81-7

Hard cover, 558 pages

**Publisher** InTech

**Published online** 01, June, 2010

**Published in print edition** June, 2010

This book is the result of inspirations and contributions from many researchers of different fields. A wide variety of research results are merged together to make this book useful for students and researchers who will take contribution for further development of the existing technology. I hope you will enjoy the book, so that my effort to bringing it together for you will be successful. In my capacity, as the Editor of this book, I would like to thank and appreciate the chapter authors, who ensured the quality of the material as well as submitting their best works. Most of the results presented in the book have already been published on international journals and appreciated in many international conferences.

### **How to reference**

In order to correctly reference this scholarly work, feel free to copy and paste the following:

Iulian Munteanu, Antoneta Iuliana Bratcu, Seddik Bacha and Daniel Roye (2010). Real-time Physical Simulation of Wind Energy Conversion Systems, Wind Power, S M Muyeen (Ed.), ISBN: 978-953-7619-81-7, InTech, Available from: <http://www.intechopen.com/books/wind-power/real-time-physical-simulation-of-wind-energy-conversion-systems>

**INTECH**  
open science | open minds

### **InTech Europe**

University Campus STeP Ri  
Slavka Krautzeka 83/A  
51000 Rijeka, Croatia  
Phone: +385 (51) 770 447  
Fax: +385 (51) 686 166  
[www.intechopen.com](http://www.intechopen.com)

### **InTech China**

Unit 405, Office Block, Hotel Equatorial Shanghai  
No.65, Yan An Road (West), Shanghai, 200040, China  
中国上海市延安西路65号上海国际贵都大饭店办公楼405单元  
Phone: +86-21-62489820  
Fax: +86-21-62489821



© 2010 The Author(s). Licensee IntechOpen. This chapter is distributed under the terms of the [Creative Commons Attribution-NonCommercial-ShareAlike-3.0 License](#), which permits use, distribution and reproduction for non-commercial purposes, provided the original is properly cited and derivative works building on this content are distributed under the same license.

IntechOpen

IntechOpen